Session 3

Coronal heating and small-scale dynamics

Courtesy Volker Bothmer 2006

https://doi.org/10.1017/S1743921306001724 Published online by Cambridge University Press

Solar Activity and its Magnetic Origin
Proceedings IAU Symposium No. 233, 2006
V. Bothmer & A. A. Hady, eds.

doi:10.1017/S1743921306001724

3D Numerical Simulations of Coronal Tectonics

I. De Moortel[1] and K. Galsgaard[2]

[1]School of Mathematics and Statistics, University of St Andrews, North Haugh, St Andrews, Fife KY16 9SS, Scotland
email: ineke@mcs.st-and.ac.uk

[2]Niels Bohr Institute, Julie Maries vej 30, 2100 Copenhagen Ø, Denmark
email: kg@astro.ku.dk

Abstract. We present the results of numerical simulations of 3D magnetic reconnection driven by photospheric footpoint motions. The model consists of two positive and two negative sources, which are placed on opposite boundaries of the cubic domain. Two different types of photospheric motions are then considered, namely rotating and twisting of the sources. These different footpoint motions result in a difference in the evolution of the magnetic skeleton and the location and efficiency of the energy build up. Both the dynamical evolution and the corresponding potential evolution of each system is investigated and a comparison is made between the energy storage and release that occurs at separators and separatrix surfaces.

Keywords. Sun: corona, magnetic fields, activity

1. Introduction

Many suggested coronal heating mechanisms rely on magnetic reconnection to convert the energy stored in the solar magnetic field into heating the local plasma. These mechanisms generally involve complex footpoint motions which slowly (compared to the local Alfvén speed) tangle and stress the coronal magnetic field. This braiding of footpoints causes a build up of magnetic energy and the formation of current concentrations, allowing reconnection to take place. In the Quiet Sun, the solar surface magnetic field is clustered in small flux concentrations, which are buffeted around by the supergranular motions and are continuously emerging, fragmenting, merging and cancelling (Schrijver & Zwaan, 2000; Parnell, 2001, 2002; Hagenaar, 2001). This magnetic carpet is continuously being replaced, due to cancellation of opposite polarity fragments and emergence of new bipolar regions and Hagenaar *et al.* (2003) estimated that the photospheric flux is recycled on a timescale of 8-19 hours. Obviously, this dynamical behaviour of the photospheric flux sources has consequences for the coronal magnetic field. The complex connectivity structure of the solar magnetic field results in the presence of many separatrix surfaces, which divide regions of different connectivity (Close *et al.*, 2004a). Developing the idea of footpoint braiding, Priest *et al.* (2002) showed that even simple motions of any one of the photospheric magnetic fragments result in the rapid formation of current sheets along these separatrix surface, enabling reconnection to occur. Hence, the connectivity of the photospheric sources changes on a timescale much faster than the photospheric recycle time. Indeed, using potential field modelling, Close *et al.* (2004b) calculated that the coronal field is recycled in as little as 1.4 hours.

Several numerical simulations have recently modelled elementary heating events, driven by simple motions of the footpoints. For example, Longcope (1998) investigated the interaction between flux sources in a constant background magnetic field and found that

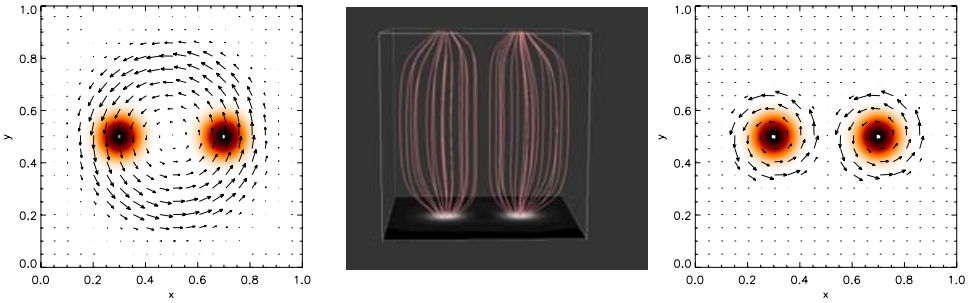

Figure 1. Contour plot of the flux sources at the bottom boundaries. The velocity vectors indicate the (left) rotational and (right) spinning driving imposed on the bottom boundary of the numerical domain. The middle figure shows the fluxtubes at $\theta = 0$.

separator current sheets form. In a series of papers Galsgaard *et al.* (2000), Parnell & Galsgaard (2004) and Galsgaard & Parnell (2005) studied similar boundary driving of flux systems and found that the two sources connect and subsequently disconnect through separator and separatrix-surface reconnection, respectively. Priest *et al.* (2005) compared the energy storage and heating that occur at separators and separatrix surfaces by considering rotating and twisting of two adjacent flux concentrations and found that coronal heating is of comparable importance at separatrices and separators.

In this paper, we present numerical simulations of both the rotating and twisting of two initially unconnected fluxtubes. The basic model and numerical setup are described briefly in Section 2 and a summary of the dynamical evolution for both drivers is given in Section 3. The current structure is described in Section 4 and the evolution of the footpoint connectivity is discussed in Section 5. Section 6 contains the conclusions.

2. Numerical Setup

The basic configuration consists of two adjacent, slender fluxtubes, which are subsequently subjected to photospheric motions. We model this situation by considering two positive sources (B_1 & B_2) on the bottom boundary and two negative sources (T_1 & T_2) on the top boundary of the cubical, numerical box (Fig. 1 - middle). The sources are aligned on the top and bottom boundaries, resulting in two distinct, straight magnetic fluxtubes. We consider two different variations of this setup, namely with and without a vertical, background magnetic field. The additional vertical field is only about 5% of the maximum field strength at the centre of the sources. The flux sources are rotated or twisted at the bottomw boundary, as shown by the velocity vectors in Fig. 1 (rotation - left; twisting - right) and the sources at the top boundary are counter-rotated (or twisted). To ease the comparison between the various experiments, we use the angle θ by which the flux sources on the bottom boundaries have been rotated (or twisted) as a reference value. Note that, as the two boundaries are counter-rotated, the fluxtubes connecting both boundaries are subject to a 'real' rotational angle of 2θ.

To follow the dynamical evolution of the 3D system, the numerical code solves the non-ideal MHD equations in a 3D, Cartesian box, which is assumed to be periodic at the sides, and bounded in the vertical direction (i.e. the direction perpendicular to the plane in which driver is situated). For a more detailed description of the numerical code, see Nordlund & Galsgaard (1997).

https://doi.org/10.1017/S1743921306001724 Published online by Cambridge University Press

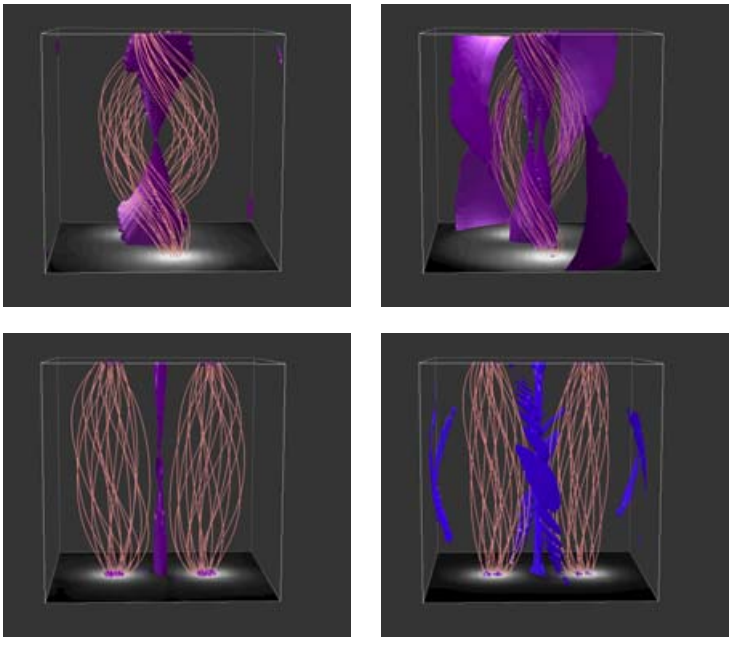

Figure 2. Fieldlines traced from the flux concentrations on the bottom boundaries at a rotational (top) or twisting (bottom) angle $\theta \approx 2$ for $B_{bg} = 0$ (left) and $B_{bg} = 0.05$ (right). The isosurfaces represent current.

3. Dynamical Evolution

When no background magnetic field is present, the numerical domain contains two separate flux domains, namely the vertical fluxtubes connecting B_1 to T_1 and B_2 to T_2, on either side of a central separatrix surface. However, when a background field is added, there are no longer distinct flux domains, as the entire boundary now contains flux of the same polarity. In this case, we define a 'fluxtube' as the volume enclosed by the fieldlines traced from a radius, r_0, from the centre of the sources (the radius of the sources in the no-background field experiment). Before the onset of the boundary driving, the fluxtubes in the $B_{bg} = 0$ experiments are in contact, unlike in the $B_{bg} \neq 0$ case, where the background field keeps the fluxtubes separated.

Driven by the boundary motions, the flux domains are forced to interact. The potential evolution of the various cases is relatively straightforward, as the potential field represents the lowest energy state. Whenever the sources on the top and bottom boundaries are aligned (i.e. at every θ that is a multiple of π), the original connectivity structure is recovered (B_1 to T_1 and B_2 to T_2). This implies that for the twisting of the sources, the potential state is at all times equal to the original configuration. When the sources are rotated on the boundaries, the flux is divided between the sources according to their relative positions, when no background field is present. When $B_{bg} \neq 0$, some of the flux will connect to the background field on the top boundary.

Fig. 2 shows a snapshot of the dynamical evolution at $\theta \approx 2$, for both the rotating (top) and twisting (bottom) drivers, and the $B_{bg} = 0$ (left) and $B_{bg} = 0.05$ (right) cases. In all the different experiments, there is a strong central current sheet (isosurfaces) and it is clear that the rotating or twisting of the sources causes the fieldlines to become increasingly twisted and tangled. The rotation or twisting of the sources causes the orientation of the fieldlines connecting the sources on the two boundaries to change

https://doi.org/10.1017/S1743921306001724 Published online by Cambridge University Press

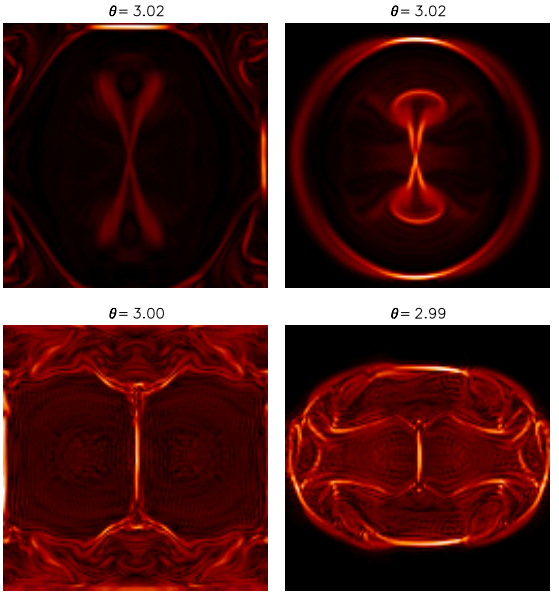

Figure 3. Contour of the current at $z = 0.5$ for (left) $B_{bg} = 0$ and (right) $B_{bg} = 0.05$ and at a rotational (top) and spinning (bottom) angle of $\theta \approx 3$.

slowly and eventually, reconnection takes places and the connectivity of the fieldlines gradually changes. When the sources are rotated, a strong tension force builds up, which initiates a stagnation point flow. On the other hand, when the sources are twisted on the boundaries, the magnetic pressure is the force that will drive the reconnection. If an additional background magnetic field is present, the onset of reconnection (between the fluxtubes) occurs slightly later compared to the no-background case, as the central flux, which keeps the fluxtubes, apart, has to be removed first, to allow reconnection between the fluxtubes to take place.

4. Current Structures

To investigate the build-up of the current structures in more detail, we focus on the central, $z = 0.5$ plane. Fig. 3 shows contours of the current at an angle $\theta = 3.0$ for the four different experiments (lighter colours correspond to higher values). When a background field is present, some of the field in the central plane is not connected to the flux sources on the boundaries and hence, is not subject to the footpoint motions. For both rotating and twisting motions, this results in a ring of current due to the shearing between rotated and non-rotated field (Fig. 3 - right). For the $B_{bg} = 0$ cases, some of the field will be almost horizontal close to the source boundaries and hence, the footpoint driving will cause large currents to build up along the periodic side-boundaries of the numerical box (Fig. 3 - left).

From Fig. 2, we saw that in all cases, a strong central current sheet builds up between the fluxtubes. Initially, in all four experiments, the sources on the boundaries are exactly aligned and hence, there are two, coinciding (quasi-)separatrix surfaces separating the flux domains. However, when the sources are rotated, these two (quasi-)separatrix surfaces will intersect at a separator, unlike in the twisting case, where the (quasi-)separatrix surfaces will remain stationary. Hence before the onset of reconnection, we can refer to the central current sheet as a 'separator' or 'separatrix' current sheet for the rotating

https://doi.org/10.1017/S1743921306001724 Published online by Cambridge University Press

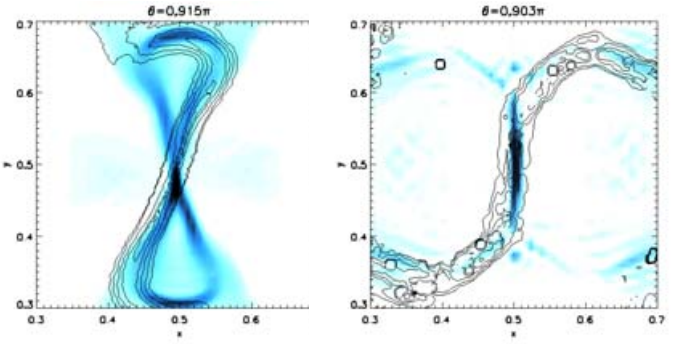

Figure 4. Contour of the current at $z = 0.5$ (central square of width 0.4) for $B_{bg} = 0.05$ and at a rotational (left) and spinning (right) angle of $\theta \approx 2.8$. The black line contours correspond to high values of the squashing factor Q.

and twisting boundary motions, respectively, as in Priest *et al.* (2005). As the footpoint motions continue, the central current sheet becomes increasingly strong, eventually allow reconnection to take place and two new flux domains are created, containing the flux connecting from B_1 to T_2 and vice versa. At this stage, there is a marked difference between the rotating and twisting footpoint motions. When the footpoints are rotated, the central current sheet bifurcates into a clear x-type configuration (Fig. 3 - top). The current structure for the twisting footpoint motions has some resemblance to an x-type structure, but with a very elongated central part (Fig. 3 - bottom). This difference is due to the different type of footpoint motions: the rotating of the flux sources results in a strong tension force toward the central part of the domain, resulting (in the $z = 0.5$ plane) in a true x-type current configuration. On the other hand, when the footpoints are twisted, there is no force driving the fieldlines toward a single point in the domain.

An additional feature in the current structure for the rotated $B_{bg} \neq 0$ case is the 'bow-like' structure on both sides of the central x-type configuration. These currents form as a result of the shearing between fieldlines associated with the flux sources and 'background' fieldlines which are also subject to the boundary driving (unlike the large ring of current, which forms due to the shearing between rotated and 'non-rotated' fieldlines). Indeed, if we look at the structure of the rotating boundary driver (Fig. 1 - left), it is clear that a substantial amount of the background field will also be subject to the boundary motions. Such current structures do not form for the corresponding twisting case, as these boundary motions are much more concentrated on the flux sources themselves, and very little of the background field is subject to the boundary driving (Fig. 1 - right).

As discussed above, when a background magnetic field is present, there are no discontinuities in the fieldline connectivity, and hence, no distinct flux domains. However, Priest & Démoulin (1995) showed that the condition of a discontinuous jump in fieldline connectivity can be weakened to a 'large' spatial variation in the connectivity. Fluxtubes which such a large variation are called *quasi-separatrix layers* (QSLs) and can be detected by measuring the *degree of squashing*, Q, where QSLs are defined as fluxtubes with large values of Q (see Titov *et al.* (2002) for a more detailed definition). Fig. 4 again shows contours of current in the central square of width 0.4 of the mid-plane ($z = 0.5$), at a rotational (left) and spinning (right) angle $\theta \approx 2.8$, with $B_{bg} = 0.05$. Overplotted are contour lines corresponding to high values of the squashing factor Q. It is clear that for both cases, strong quasi-separatrix layers build up, and that the currents do indeed build up along the QSL's. Hence, in both the $B_{bg} = 0$ and $B_{bg} \neq 0$ case, and for both types of footpoint motions, currents build up in region of strong shear in magnetic connectivity.

https://doi.org/10.1017/S1743921306001724 Published online by Cambridge University Press

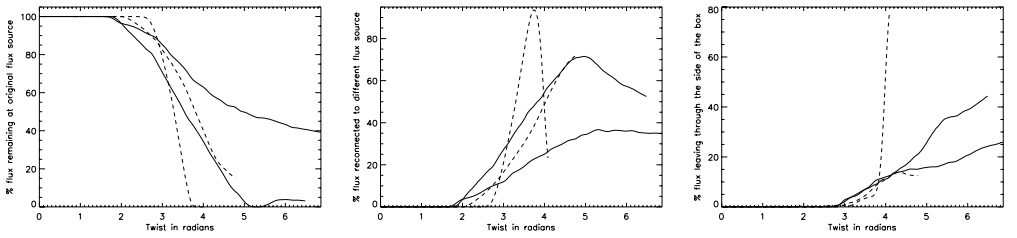

Figure 5. The evolution of the flux, as a percentage of the total flux in the source, (left) remaining at the original connection, (middle) reconnected to a different source and (right) the flux associated with fieldlines leaving the sides of numerical box or connecting to parts of the top boundary not associated with the flux concentrations. Solid and dashed lines correspond to the twisting and rotating boundary driving, whereas the thick and thin lines correspond to $B_{bg} = 0$ and $B_{bg} = 0.05$, respectively.

Only part of the structure is visible in the Q-values in Fig. 4 as the tracing of the fieldlines, on which the determination of Q is based, was only done in one direction (from the mid-plane to the top boundary). Fig. 4 also clearly shows that the QSL's will form a true x-type configuration, intersecting at a single point for the rotational driving. For the twisting of the flux sources, the QSL's partially coincide, resulting in the elongated current structure in the central part of the $z = 0.5$ plane.

5. Connectivity Evolution

To study the changes in connectivity and the amount of flux associated with them, we follow the method of Parnell & Galsgaard (2004): during the footpoint driving, the shape of the flux sources is mostly maintained and hence, a fixed amount of magnetic flux can be associated with each traced fieldline. To investigate the evolution of the footpoint connectivity, we trace a large number of fieldlines from the flux sources on the bottom boundary of the numerical domain. As the fieldline connectivity evolves, the amount of 'reconnected' flux can be determined. Fig. 5 shows the evolution of the amount of flux, as a percentage of the total flux at that source, which is (left) still at its original connection, (middle) connected to the other source on the top boundary or (right) at a different connection (parts of the top boundary not associated with the flux concentrations or connecting to the neighbouring (periodic) domain). The evolution of the magnetic flux is show both for the rotating (dashed lines) and the twisting (solid lines) of the sources and for the $B_{bg} = 0$ (red lines) and $B_{bg} = 0.05$ (black lines) cases.

As expected, Fig. 5 shows that the onset of reconnection between the two fluxtubes occurs at larger values of the angle θ, when a background field is present; this background field initially separates the fluxtubes and has to be removed before the fluxtubes come into contact. The difference in the onset of reconnection between the $B_{bg} = 0$ and $B_{bg} \neq 0$ case seems more pronounced for the rotational driving of the magnetic sources. At the same time, reconnection is clearly faster when a background magnetic field is added, as the flux density will be higher when the fluxtubes enter the central current sheet. For both types of footpoint driving, 100% of the flux has reconnected before the end of the experiments in the $B_{bg} \neq 0$ cases, whereas only $\pm 60\%$ of flux has reconnected in the final stage of the twisted $B_{bg} = 0$ case. The very rapid increase in the flux not connected to either of the flux sources for the rotated $B_{bg} \neq 0$ case (Fig. 5 - right, dashed black line) occurs when the outward propagating 'bow' currents collide with the current of the sides of the numerical domain, allowing a large amount of fieldlines to connect

https://doi.org/10.1017/S1743921306001724 Published online by Cambridge University Press

to the neighbouring domains. Finally, we note that reconnection between the fluxtubes appears to start slightly earlier when twisting, rather than rotating, the magnetic flux concentrations.

6. Discussion & Conclusions

We have presented a brief summary of the results of 3D numerical simulations of magnetic reconnection driven by simple footpoint motions. Despite the fact that the various experiments represent substantially different topological situations, the overall, dynamical evolution of the four cases showed many similarities. The initial setup consist of two adjacent, straight fluxtubes, connecting two positive and negative sources on the top and bottom boundaries of the numerical domain. Two variations of this basic model are considered, namely with and without and additional vertical background magnetic field. This setup results in two central, initially coinciding (quasi-)separatrix surfaces. Subsequently, the footpoints of the fluxtubes are subjected to either rotating or twisting motions. As suggested by the tectonics model of Priest *et al.* (2002), these simple footpoint motions lead to a rapid build up of current sheets along the (quasi-)separatrix surfaces. Indeed, determining the values of the squashing-degree Q confirmed that the highest currents are concentrated along the quasi-separatrix surfaces, where there is a strong shear in magnetic connectivity. The tension forces created by the rotational driving of the flux sources resulted in a clear, central x-type configuration, which is the case when the flux sources are twisted on the boundaries.

The evolution of the footpoint connectivity happens in a non-trivial manner and shows very little resemblance to the cyclical nature of the corresponding potential connectivity evolution. At the start of the experiments, the additional background field confines the fluxtubes and has to be removed before the fluxtubes can come into contact at the central current sheet. Hence, in the $B_{bg} \neq 0$ case, the flux sources have to be rotated or twisted over a larger angle before reconnection between the fluxtubes takes place. However, this also leads to higher concentrations of flux density at the onset of reconnection and hence, a faster rate of reconnection than in the $B_{bg} = 0$ cases. The onset of reconnection occurred at slightly smaller angle ($\theta = 0.47\pi - 0.59\pi$) for the twisting of the footpoints, compared to the rotational driving ($\theta = 0.65\pi - 0.78\pi$), regardless of the value of the background magnetic field.

The numerical experiments presented in this paper were designed to study 3D magnetic reconnection driven by very simple footpoint motions. Many aspects of these numerical simulations remain to be investigated further and for a more comprehensive and detailed description of the analysis and results presented here, we refer the reader to De Moortel & Galsgaard (2006a, 2006b). As the experiments have some significant shortcomings, a direct comparison with realistic, solar situations is not relevant. For example, the initial atmosphere contains a constant pressure and hence, values of the plasma β are much higher than expected in the solar corona. This could be addressed by including gravity but this is not expected to influence the global, dynamical evolution significantly. Furthermore, the initially symmetrical position of the flux sources on the top and bottom boundary is probably not realistic and should be replaced by flux concentrations that are non-aligned, even before the start of the boundary driving.

The periodic boundary conditions at the sides of the numerical box can be considered to be an additional shortcoming. As it allows the fieldlines to connect to the neighbouring periodic domain, it significantly complicates the dynamical evolution, especially in the later stages of the experiments. When no confining background magnetic field is present, some flux reconnects through the boundaries throughout the experiment. However, at

https://doi.org/10.1017/S1743921306001724 Published online by Cambridge University Press

the same time, this periodic setup can be seen as more realistic than an isolated numerical domain, as the photospheric magnetic carpet is full of flux concentrations. In the context of the coronal tectonics model of Priest *et al.* (2002), coronal loops connect to the photosphere in a multitude of different magnetic fragments. The two fluxtubes in our experiments can be seen as two individual loops strands, with the loop strands in the neighbouring domains making up the rest of the coronal loop. Hence, it is more naturally to allow not only for interactions between the fluxtubes inside the numerical domain, but also with the surrounding loops strands through the periodic boundary conditions.

Acknowledgements

IDM acknowledges support of a Royal Society University Research Fellowship. KG was supported by the Carlsberg Foundation in the form of a fellowship.

References

Close, R.M., Parnell, C.E., & Priest, E.R., 2004a, Sol. Phys.225, 21
Close, R.M., Parnell, C.E., Longcope, D.W., & Priest, E.R., 2004b, ApJ 612, L81
De Moortel, I., & Galsgaard, K., 2006a, A & A, *in press.*
De Moortel, I., & Galsgaard, K., 2006b, A & A, *submitted*
Galsgaard, K., Parnell, C.E., & Blaizot, J., 2000, A & A 362, 395
Galsgaard, K., & Parnell, C.E., 2005, A & A 439, 335
Hagenaar, H.J., 2001, ApJ 555, 448
Hagenaar, H.J., Schrijver, C.J., & Title, A.M., ApJ 584, 1107
Longcope, D.W., 1998, ApJ 507, 650
Nordlund, A., & Galsgaard, K., 1997, *A 3D MHD code for Parallel Computers*, Technical report, Astronomical Observatory, Copenhagen University
Parnell, C.E., 2001, Sol. Phys. 200, 23
Parnell, C.E., 2002, Mon. Not. Roy. Astron. Soc. 335, 389
Parnell, C.E., & Galsgaard, K., 2004, A & A 428, 595
Priest, E.R., & Démoulin, P., 1995, J. Geophys. Res. 100 A12, 23443
Priest, E.R., Heyvaerts, J.F., & Title, A.M., 2002, ApJ 576, 533
Priest, E.R., Longcope, D.W., & Heyvaerts, J.F., 2005, ApJ 624, 1057
Schrijver, C.J., Zwaan C., 2000, *Solar and Stellar Magnetic Activity* (Cambridge; Cambridge Univ. Press)
Titov, V.S., Hornig, G., & Démoulin, P., 2002, J. Geophy. Res. 107 A8, 3-1